Extension and Experimental Verification of a New 'First Contact' Method to Model Performance of Multilayer Contact Interfaces

Marjorie Myers, Michael Leidner, Helge Schmidt – Tyco Electronics,
Helmut Schlaak - Darmstadt University of Technology – Institute for Electromechanical Design

***Abstract*— As the connector industry moves towards the use of smaller and smaller contact designs, achievable contact normal forces have been reduced to levels below what has been typically used previously in connector applications. Therefore, improving the ability to predict and analyze the mechanical and electrical performance of these lower force contact interfaces is becoming increasingly important. This paper will illustrate further development and experimental verification of a new method to simulate elastic/plastic contact between two multi-layered non-conforming rough surfaces. This new approach involves using six scale independent parameters to statistically model two 3-dimensional multilayered surfaces coming into contact. The mechanical and electrical response characteristics of all the layer materials, as well as frictional behavior at the contacting asperity surfaces, are taken into account as pressure is applied between the surfaces and the a-spot distribution is formed. The mechanical and electrical contact performance of the resulting interface are calculated and visualized in 3 dimensions. The model has been extended and applied to contacts with varying surface finish materials and surface topology characteristics. These results are then compared to experimental data generated from samples with comparable finishes.**

***Index Terms*—a-spot distribution, constriction resistance, contact resistance, modeling**

I. Introduction

The mechanical response and contact resistance between two multilayer non-conforming mating surfaces can be complex. The work of Holm [1] and Hertz [2] are widely used in connector design, but their models can be limited due to phenomena they are not able to incorporate [3] [4] [5]. Traditional Finite Element Modeling (FEM) techniques are also inherently limited due to the complexity of contact interface surfaces. FEM solutions for a single asperity [6] or a collection of asperities [7] are not capable of predicting realistic topography effects. Leidner et al [8] [9] describe a 3 dimensional model incorporated into a program called 'First Contact' which uses a new approach to simulate the electrical and mechanical performance of contact interfaces. A detailed description and further references can be found in references 8 and 9. Therefore only a brief description will be given here since the focus of this paper is to validate the model.

A. Model of the Surface Topographies

This model can use either measured surface topographies or numerically simulated surface topographies. Fast terrain mapping procedures [10], or approaches that take the self affinity (fractal behavior) [11] of technical surfaces into account; do not offer a straightforward way to create anisotropic features.

The engineered surfaces used in connector applications typically have anisotropic features such as rolling marks. Therefore, a statistical approach using a Finite Impulse Response (FIR) filter [12] [13] was used to model anisotropic connector surface topographies. It has been shown that engineered surface topographies can be modeled using 6 independent scale parameters: root means square (RMS) roughness, either a linear or an exponential form of the auto correlation function (ACF), x/y correlation length, skew, and kurtosis. The correlation between the simulated surfaces and comparable measured surfaces has been demonstrated [8] [9] (Figure 1). The model can also accommodate varying surface geometries.

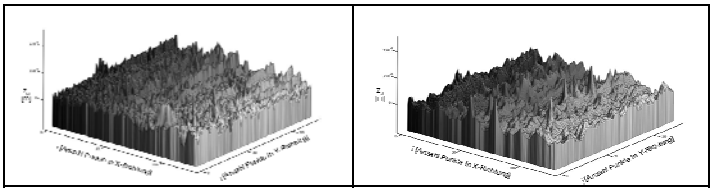

a) measured | b. simulated

Figure 1: Measured and a comparable simulated surface topography for a Au plated contact surface (see Table 4 for parameter details); RMS roughness σ=0.28 μm; X/Y resolution 128 x 128 points; 1.56 μm/point.

An x/y resolution of 128 x 128 points leads to reasonable computing times without sacrificing accuracy. A 0.8 μm point resolution is used for analysis in the range of 1 – 50 cN. For a greater load range of 1-250 cN, it was necessary to use a coarser 1.56 μm point resolution. This was done by removing every other data point from the 3 dimensional surface topography files. This results in a simulated contact interface with fewer and larger a-spots available for current conduction. The 'Electro Solver' portion of the model used to calculate the contact resistance would be more sensitive to this decrease in resolution at the lowest loads.

Manuscript received May 16, 2008

B. *Generation of the Contact Interface A-spot Distribution*

This model uses a numerical algorithm to calculate the stresses and deformations that occur in response to an applied load in a contact system with up to three different layers per contacting surface [8] [9] (Figures 2 and 3). Either measured or simulated surface topographies can be applied.

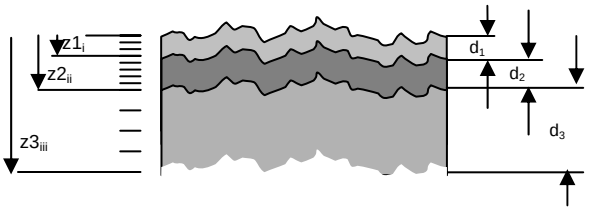

Figure 2: Two dimensional schematic showing morphology of the layers within the model.

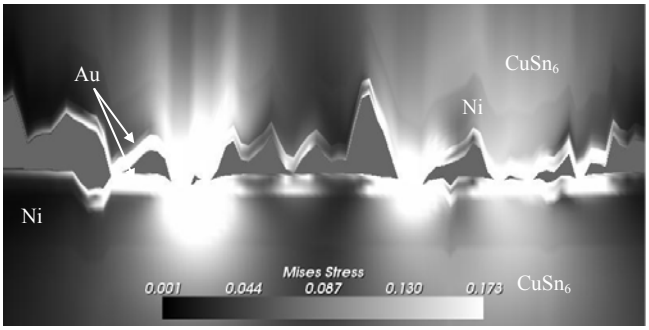

Figure 3: 'First Contact' grey scale map of the von Mises stress distribution through the contact interface for the standard Au sample.

Only dry, un-lubricated, clean surfaces are used. Only normal and shear traction are considered. Adhesion forces due to meniscus forces and/or adhesion energy [14] are neglected. Each layer is assumed to have a uniform thickness and all the layers have identical topographies. The substrate/bulk material is represented as one of the layers. The plastic deformation of the individual contact points (a-spots) can be interpolated using different material hardening behaviors. The hardening behavior used in this work is shown in Equation (1) [9].

$$H^{eff}(p) = \begin{cases} p; & if\ p < Y_{eff} \\ \dfrac{Y_{eff} + P}{2}; & if\ Y_{eff} \le p < 2Y_{eff} \\ Y_{eff} + \dfrac{p}{4}; & if\ p \ge 2Y_{eff} \end{cases} \quad (1)$$

$H^{eff}(p)$ denotes the effective hardness as a function of the point load p and the effective yield stress, $Y_{eff} = 3Y$; where Y is the minimum Yield Strength of the two contact partners [15]. The x and y coordinates in Equation (1) are omitted for brevity.

The model is based on the use of Papkovich Neuber Potentials [16] [17] and both multi-grid and conjugate gradient methods [18]. An analytical solution for the 9 independent coefficients for the case of a two layer system (e.g., Hot Air Leveled Sn (HAL Sn) over CuSn6 Phosphor Bronze) can be found in the literature [16] [17]. An analytical solution for the 15 independent coefficients of a three layer system has not been found in the literature. This model uses an alternative numerical approach to solve a three layer equation system, (e.g. a Gauss Seidel algorithm) where appropriate auxiliary conditions are applied. An iterative process is used to generate the a-spot distribution/area of the contact interface incorporating the mechanical response characteristics of the mating layered material systems [8] [9]. Figure 4 shows examples of a-spot distributions generated by the model with increasing load for standard hard Au over Ni over Phosphor Bronze contact interface.

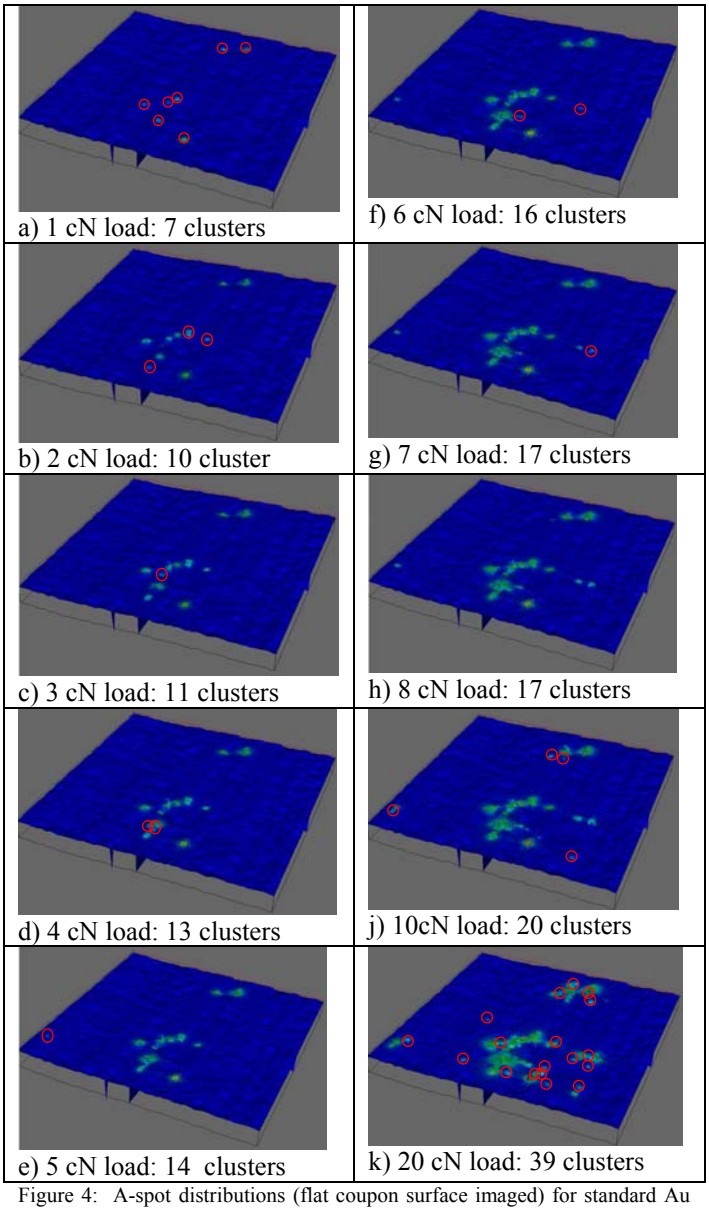

Figure 4: A-spot distributions (flat coupon surface imaged) for standard Au contact interfaces at various loads; X/Y resolution 128 x 128 points; 1.56 µm/point (circles denote new clusters appearing with increasing load).

C. *Contact Resistance Calculation*

At this point, current can be applied to the system, the potential drop across the a-spot distribution/area can be obtained, and the interface resistance can be calculated. The determination of the potential drop through the contact interface is done by solving the Laplace equation using a Gauss Seidel iterative scheme [8] [9]. Figure 5 illustrates the potential drop within a cross section through a standard Au

contact interface. The two main routes are due to the existence of two separate clusters of a-spots. This method can incorporate both the resistance properties of the individual layers and any interactions among current paths.

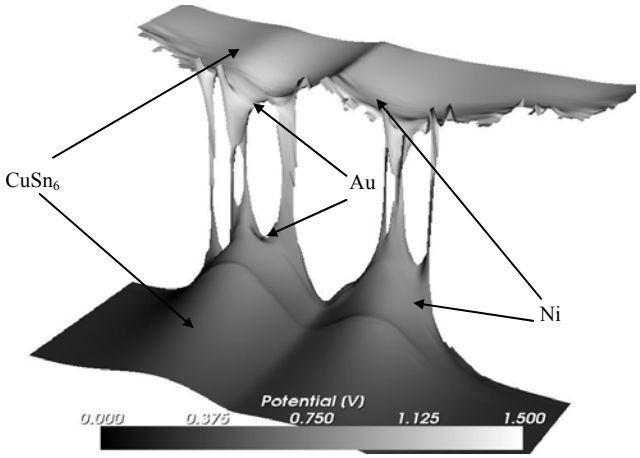

Figure 5: 'First Contact' x/z cross-sectional view taken across a Au contact interface showing potential values represented as grey scale and height.

II. SAMPLES AND EQUIPMENT/TESTING PROCEDURES

A. *Samples*

To experimentally generate data to verify the results of the model, comparably finished standard flat coupon/hemispherical cap (nominal radius 2.5 mm) contact pairs were tested. They were designed and produced to have material and surface qualities of a typical separable connector contact mating a stamped surface (coupon) to a formed surface (cap). All the samples were made from 0.4 mm thick H04 temper C51100 phosphor bronze (CuSn4) rolled strip. Standard connector industry high speed reel-to-reel production dies and plating processes were used to stamp, form, and plate the coupons and caps on separate reels. The one exception is the polished smooth Au samples which were made from a custom ordered reel of production rolled stock material. The caps were individually formed from the flat stock using comparable hand tooling, electro-polished, and then laboratory plated. This enabled surface qualities different than would be typically made in a production environment. All the samples used in this work had a Ni underplate. Tables 1-4 lists the relevant sample parameters for the samples used in this work.

Table 1: Specific contact material parameters

Material	Au (Co hard)	Ag	Sn (matte)	Ni (underplate)	CuSn6 (C51100)
E [GPa]	78	82	49.9	199	112
Y [MPa]	200	120	14.4	660	560
ρ [Ωm]	2.2	1.63	12.6	6.9	12.28

E modulus of elasticity, Y Yield strength, ρ specific resistance

Each sample was ultrasonically cleaned for 30 seconds in 2-propanol followed by 24 – 48 hours lab atmosphere drying prior to contact resistance measurement. All testing was performed on samples in such an un-lubricated, dry, cleaned state.

Table 2: Contact layer thicknesses * [µm]

Layer	Top layer		Nickel Underplate	
	cap	flat	cap	flat
Standard Au	0.38	0.38	1.27	1.27
Smooth Au	0.38	0.38	1.27	1.27
Ag	2.39	2.38	1.63	1.6
Ag/Thin Sn	1.09 (Sn)	2.38 (Ag)	1.91	1.6
Thin Sn	1.09	0.79	1.91	1.27
Thick Sn	3.25	2.64	1.91	1.27

* model bulk material thickness 12µm

Table 3: Topography roughness parameters

RMS Roughness		Standard surface	Smooth surface	Simulated		
σ [micrometers]	Cap	0.25	0.12	0.002	0.02	0.2
	Flat	0.47	0.043	0.002	0.02	0.2

Table 4: Topography simulation parameters

	ACF	β_x [pts]	β_y [pts]	skew	kurtosis
Cap	expo.	20	2	0	3
flat	expo.	2	2	0	3
Figure 1 b.	expo.	6	6	0.88	7.17

The Au and Sn plated samples were stored on reels under lab atmosphere conditions after plating prior to testing because they typically won't form tarnish films. The Ag samples were stored on reels with sulfur-free interleaving paper, wrapped in 'silver saver' paper (designed to adsorb hydrogen sulfide and other sulfurous gases), in closed plastic bags. This does not eliminate exposure to sulfur completely, but it does attenuate it. The parts were openly exposed to a plating plant atmosphere just after plating and before packaging; and lab atmosphere during cleaning, drying, and measuring.

B. *Contact Resistance Probe (CRP):*

The CRP is a computer controlled instrument used to make contact resistance measurements at varying normal loads. Each individual contact resistance measurement is an average of a series of readings made under both forward and reverse current DC steady-state 4-wire dry circuit (50mA/50mV limited) conditions. All measurements are taken under lab atmosphere conditions. The process is load controlled and has a minimum resolution of 0.1 cN. The instrument is capable of incorporating wipe into the measurement routine, as well as taking measurements during the unloading process; those options were not used in this work. When using the standard flat/cap sample configurations, a maximum of 18 measurements can be made with each cap. The instrument can be adapted to work with non standard coupon/cap parts.

The coupon of a mating half is mounted to the X/Y table with an incorporated load cell. The current-out and voltage-out leads are attached to opposing sides of the mounted flat coupon. The hemispherical cap is mounted to the tip of the probe head which can move in the vertical z direction. This probe head holds the cap at an angle so that successive measurements can be taken using the same cap by rotating the head to present a 'fresh' location to the opposing mating flat coupon surface. The current-in connection is made at the outer rim of the cap and the voltage-in lead makes contact at the bottom of the back of the 'cup' of the cap. Figure 6 shows a

picture of a Au plated cap mounted to the probe head and an Au plated flat mounted on the x/y table, as well the current and voltage measurement locations.

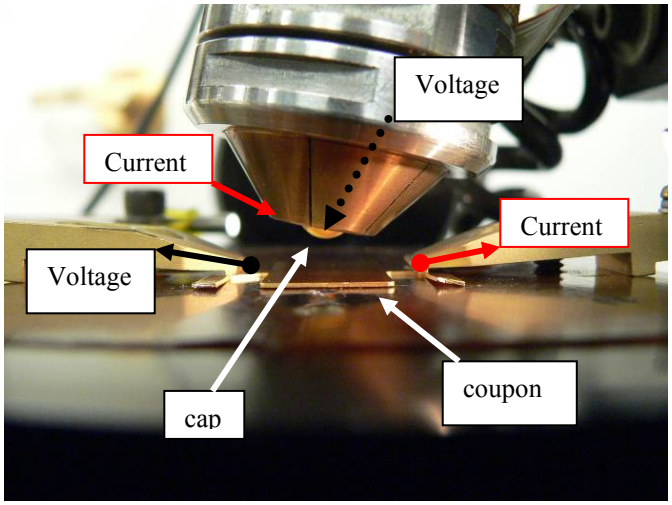

Figure 6: Image of the CRP instrument and sample orientation.

The measurement process starts by specifying the measurement routine, specifying the area on the coupon to be tested, zeroing and calibrating the load cell, then 'finding the surface' as the head is brought towards the flat surface until a load of 0.1 cN registers on the X/Y table load cell. Then the measurement routine starts. The load is monotonically increased with pauses to collect the contact resistance data. When the final load is reached and the final measurement is taken for a particular contact interface reading, the head raises up away from the flat coupon surface. The X/Y table indexes to the next measurement location, the head rotates to a fresh spot on the hemispherical cap, and the process starts from the surface sensing step for as many times as was prescribed in the measurement routine.

III. Results and Discussion – Measured vs. Model Data

A. The Spread in the Data

Figure 7 is a log/log plot showing multiple measured contact resistance data curves for the standard Co hardened Au over Ni plated contact pair being loaded from 1 – 50 cN.

'Clean' contact surfaces existing in our 'real' world atmospheres will have unavoidable adsorbed films that the 'model' world does not include. Factors such as these adsorbed films [19], tarnish films [1], and variability in localized surface roughness and plating thicknesses within the sample measurement regions could contribute to the variability in the measured data. Variability in surface roughness across the measurement area can be incorporated in the model directly, but adsorbed and tarnish films have to be handled in an indirect manner.

Model data was generated using both the measured surface topography from the samples tested, as well as numerically simulated topographies. Since the model only calculates the constriction resistance occurring at the contact interface, a constant equipment/sample specific offset resistance (R_{offset} = 0.8 mΩ) is included in the model to compensate for any bulk resistance included in the measurement coming from equipment/sample geometry limitations.

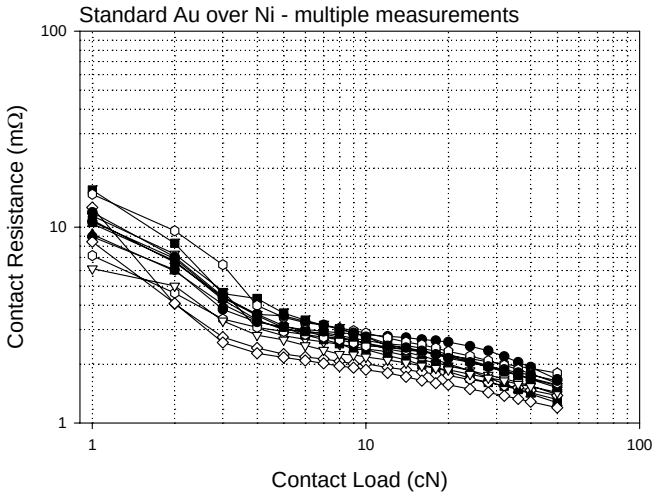

Figure 7: Multiple representative measured contact resistance curves for mated Standard Au over Ni surfaces.

Figure 8 is another log/log plot showing the same data in a median, maximum, and minimum format with the various forms of model output superimposed.

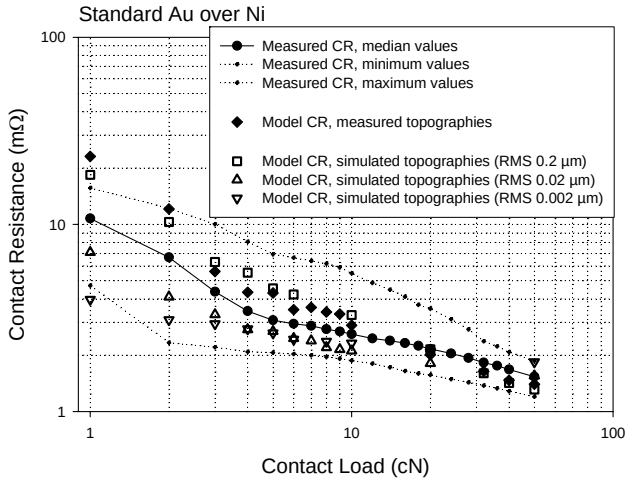

Figure 8: Contact resistance data for a Standard Au over Ni sample pair – as well as model results using the measured topography and simulated topography with varied RMS surface roughness values (0.2, 0.02 and 0.002 µm).

Model results generated using measured standard Au coupon and cap surface topographies show very good agreement in both range and trend with the measured standard Au median data (Figures 7 and 8) [9]. Comparable simulated model topographies were used to generate data where the surface roughness was varied from the measured topography value to illustrate what effect such variation would have (Figure 8). The level of overall resistance stayed within the range of the measured standard Au data, but the trends deviate when the RMS roughness approaches significantly lower values (*e.g.*, 0.002 µm). This variation will be discussed in a later section.

B. Alternative Finish Material and Tarnish Films

This correlation in range and trend between the model and measured median data can also be seen when comparing data for mated Ag plated samples (Figure 9). The deviation of the model trend from the median measured values as the load increases above ~ 100 cN will be discussed in a later section. The variability in the measured data for the Ag samples is significantly greater than for the Au samples. This would be expected due to the fact that atmospherically exposed Ag surfaces will form a non-uniform tarnish film [20] [21] in addition to any adsorbed films. Au does not form tarnish films in response to typical atmospheric exposure and is generally limited to any adsorbed films.

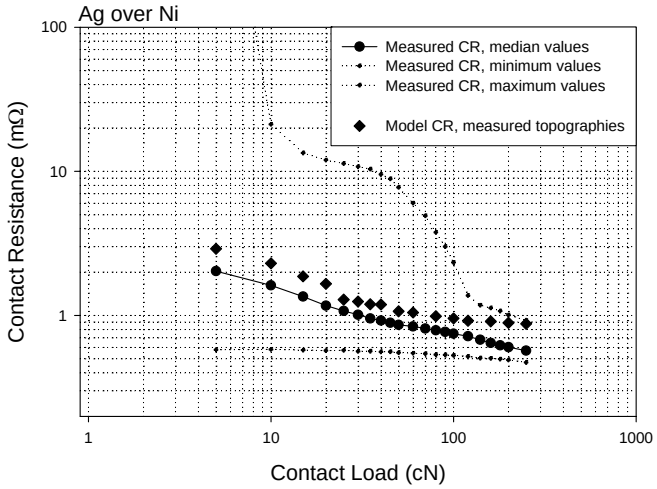

Figure 9: Measured contact resistance data compared to model results for a Ag over Ni plated contact pair being loaded from 1 – 250 cN.

C. The 'Knee' in the Data

There is a two slope/transition 'knee' trend in the log/log plot of the contact resistance data occurring in the range of 10 – 15 cN load (e.g., Figures 7 and 8). This occurs in both the measured data and the model results, but differs from the single slope log/log fit predicted using the traditional analysis:

$$R_C \approx const \cdot F_N^{-n} \qquad (3)$$

This phenomenon has been observed for the different finishes in our work and in work done more on the level of microelectromechanical systems (MEMS) applications [22]. The load range and contact dimensions in MEMS applications are an order or two of magnitude lower than what is used in connector applications (Figure 10). A correlation can be made between the two types of data due to the fractal nature of engineered surfaces.

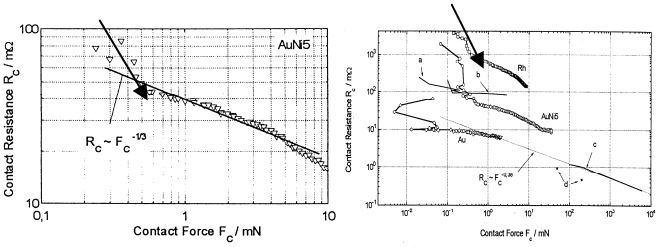

Figure 10: Measured 'knee' effect in micro contact measurements [23].

Using this model, a possible explanation can be illustrated. J. A. Greenwood [5] developed an approximate theoretical representation of the resistance (R_E) associated with current being redistributed through an array of a-spots within a contact interface (ρ = resistivity, a = circular a-spot area, s = distance between a-spots).

$$R_E = \frac{\rho}{2\sum a_i} + \frac{\rho}{\pi}\frac{\left(\sum\sum \frac{a_i a_j}{s_{ij}}\right)}{\left(\sum a_i\right)^2} \qquad i \neq j \qquad (2)$$

Such a simplified model is difficult to apply to 'real world' 3 dimensional multilayer contact interfaces. In the present model, the plastic response and the 3-dimensional composite material structure of the surfaces being brought together are incorporated. Therefore the a-spot size and relative position distributions (individual and cluster) are generated. Therefore, the evolution of the individual current paths within the contact interface at each load can be simulated and the contact resistance calculated.

In reality, the mechanical stresses developed at the individual asperity junctions are sufficiently high to cause the material response at those asperities to be effectively fully plastic [24]; especially at the load ranges used in this work. This can be illustrated by the fact that a log/log plot of the number of a-spots vs. contact load follows the power law as per equation (2) (Figure 11). If an elasto-plastic transition would be detectable, this curve would not be logarithmic in this load range.

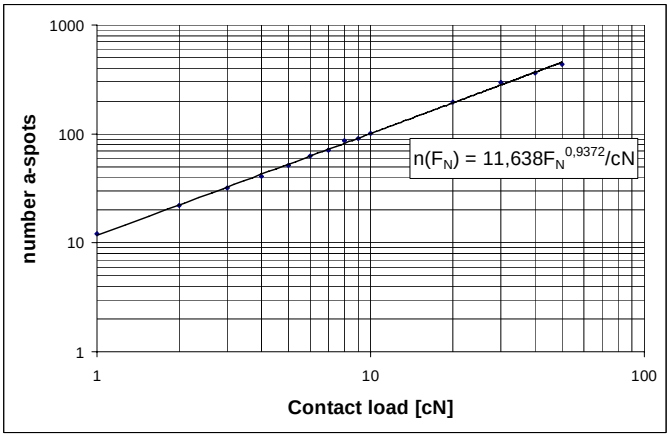

Figure 11: Model results illustrating how the number of a-spots correlates to increasing contact load 1 – 50 cN for the Standard Au over Ni plated samples.

The distribution of the current within the contact interface is dependant on both the spatial distribution of the a-spots, and magnitude of current passing through each a-spot [5]. The amount of current being passed through each individual a-spot current path is related to the magnitude of the individual a-spot area. The larger the a-spot area, the larger the fraction of the total current is passed through that current path.

This 'knee' transition is therefore, dependant on the evolution of the a-spot distribution – both the spatial proximity and the a-spot area size distributions. How the a-

spot distributions develop is dictated by how the macro (sample surface geometries) and micro (surface roughness) of the two impinging surfaces interact.

At initial loading, all the new individual a-spots develop in disparate regions within the contact area. Preferential spatial clustering of newly generated a-spots becomes evident with increasing load (Figure 4). As load increases, any new a-spots tend to preferentially form, or cluster; in regions dictated by how the two surface geometries interact (Figure 4). That is not to say that the development of new a-spots is attenuated (Figure 11). As the a-spot clustering develops, new a-spots added to the contact interface as the load is increased further have a diminishing effect on how the current is distributed across the contact interface. The proximity distribution (degree of clustering) of the newly developing a-spots will not change dramatically after the clustering of a-spots has developed. Effectively, the resistance distribution within the contact interface to approaches a constant level. This can be seen by how the a-spot distribution develops and in the transition of the measured and modeled contact resistance curves to the second slope region (Figures 8 and 9).

Initial Slope Deviation of the Model from the Measured Data

The model data in the initial low load slope/transition 'knee' region tends to be higher than that of the measured data (Figure 8). Unlike the algorithm used to calculate the deformation of the a-spots, the 'Electro-solver' portion of the model used to calculate the contact resistance is limited to a constant mesh size. Therefore the size of an a-spot subjected to different pressures does not vary. Especially at the beginning of the mating process, individual a-spots have to bear higher loads than additional a-spots at the rim of an a-spot cluster. In addition, the heating and softening of an individual a-spot is not yet implemented into the model. Hence at very low loads a higher interface resistance output would be reasonable in the model results.

Shifting of the' Knee' – 'Rough' vs. 'Smooth'

One way to shift this 'knee' would be to shift the a-spot proximities and distribution. One way to do this would be to measure and model contact of samples with similar geometry but significantly different asperity distributions (*e.g,*. surface roughness). This was done numerically using the model and experimentally with available samples. Figure 12 shows measured median, maximum and minimum contact resistance curves for the smooth Au samples. It also includes a set of model data generated using measured topography from the polished smooth surfaces. The model results were then re-generated using a comparable simulated surface with the RMS roughness adjusted down to 0.002 micrometers; two orders of magnitude lower than the standard Au sample data.

The most prominent difference seen when comparing these standard and smooth data curves (both measured and model) is that the 'knee' tends to decrease in magnitude, and all but 'disappear' with decreasing RMS surface roughness. This transition with decreasing roughness can also be seen in the model results in Figure 8. This attenuation of the initial slope region in the low load region occurs at lower RMS surface roughness values for the model data than the measured data, but the model is still able to reproduce the effect on the order of the measured contact resistance data range.

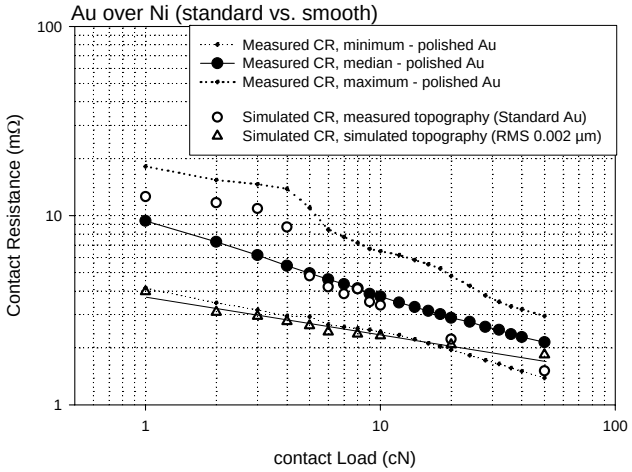

Figure 12: Polished smooth Au measured data compared to Standard Au model results, as well as corresponding simulated surface topography model results generated by reducing the RMS roughness to 0.002 µm.

The total amount of area generated to support a given load is the same for the smooth vs. the standard surfaces. The difference is in how and when clustering occurs (Figure 13). For the smoother surfaces, the clustered nature of the contact interface is less widely distributed, more uniform, and predominates at correspondingly lower loads due to the more uniform nature of the surface.

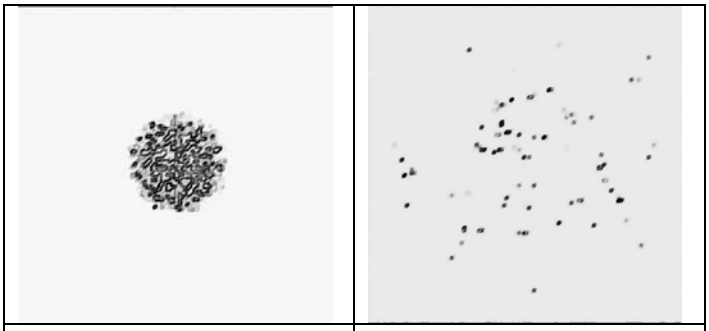

Figure 13: The difference in a-spot distribution clustering between a 'relatively smooth' Au surface and a 'standard' Au surface at a load of 100 cN.

Producing contacts with a surface roughness quality of this magnitude is not practical for the bulk of connector applications, but it does illustrate the effect the initial evolution of the contact interface has on the contact resistance values. Figure 13 can also be used to illustrate that for the case of very smooth surfaces, such as MEMS contacts (Figure 10), the 'knee' appears at the corresponding lower load magnitudes.

D. Adding an Inherent Oxide Layer- Sn

This model is designed to work with clean surfaces. Sn (pure Sn) platings develop a relatively self-limiting oxide film when exposed to typical atmospheric conditions. A way to compensate for such a film within the model would be to

incorporate a minimum 2 GPa 'threshold' pressure that is greater than the yield strength of the contacting surface metal materials. That would establish a minimum pressure required to crack the oxide layer and extrude fresh Sn metal to make metallic contact [25]. That is a pressure below which good metallic contact would not occur as each a-spot develops with increasing load. Figure 14 shows measured contact resistance data for thin Sn over Ni contact interfaces; as well as measured surface topography model results, with and without the 'threshold' adjustment. The 'threshold' adjusted data correlates quite well with the measured median data.

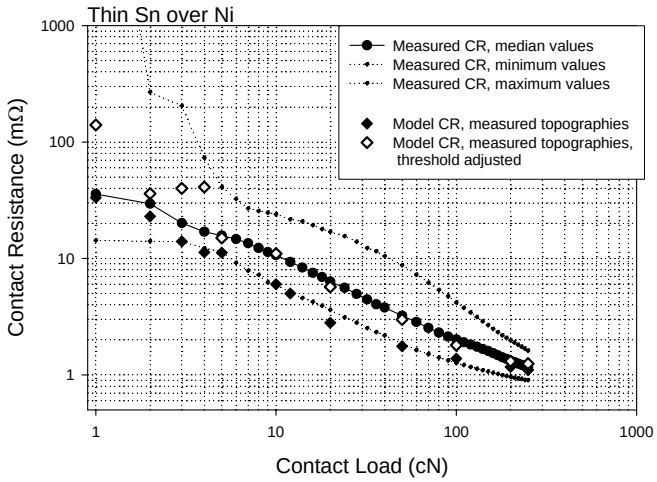

Figure 14: Measured contact resistance data compared to model results for a thin Sn contact interface – with and without the threshold adjustment.

Thick vs. Thin Platings: Limitation

The next step was to extend this analysis to the thick Sn measured sample data. Figure 15 shows the measured results along with the model results using the measured topography and the coarser resolution. The data matches very well with the median of the measured data without the 'threshold' adjustment. This could be due to differences in the composite hardness of the material supporting the load between the surfaces in conjunction with limitations in the boundary conditions of the model.

The composite hardness of the material supporting the load between the surfaces is significantly less for the thicker Sn samples than with the thin Sn samples because the volume of material deforming to support the load between the surfaces has a significantly larger fraction of relatively soft Sn rather than the harder supporting Ni and Cu alloy [26]. Therefore, the elastic/plastic deformation zone extends further into the substrates as the two surfaces move deeper into one another. This leads to greater plastic flow of material, greater oxide cracking/breakup, more extrusion of soft Sn at the surface, generation of a larger area of metallic contact, and a lower constriction resistance at the interface – in direct opposition to the effect of having the oxide at the interface. Therefore, the applicability of this 'threshold' adjustment is less clear in this case.

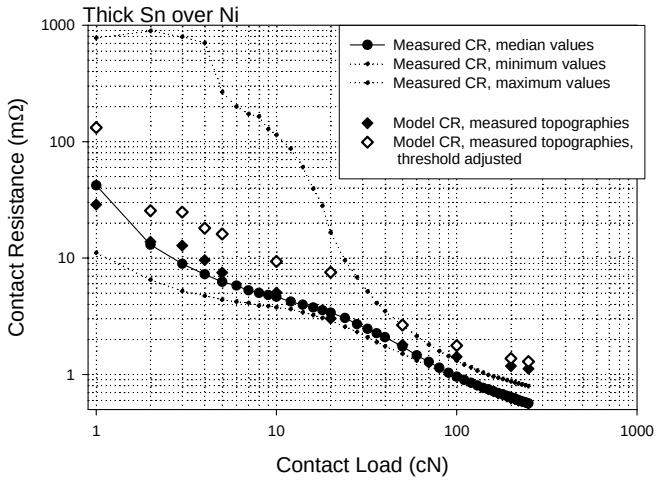

Figure 15: Measured contact resistance data compared to model results for a thick Sn contact interface – with and without the threshold adjustment.

In the 'real' world, when the plastic deformation zone in and around the contact interface reaches the surface, material will flow away from the contact interface junctions 'out-of-plane' and into the spaces between the two surfaces. This type of material flow is not currently incorporated into the model (Figure 16). At the higher loads, this would lead to a modeled a-spot distribution with an unrealistically small area of real contact and higher contact resistance calculations. This trend can be seen at loads ~ 100 cN and higher for the model data where the thicker coatings are being mated (Figures 9 and 16).

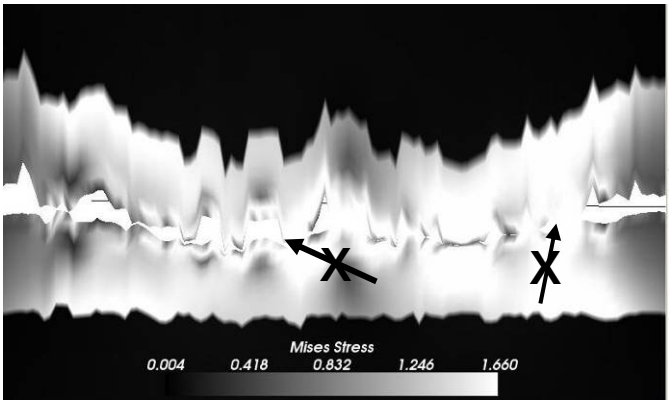

Figure 16: Illustration of lack of out-of-surface material flow in the model – von Mises stress cross-section across the model thick Sn contact interface.

This limits the ability of the model to represent the a-spot development process for these thicker samples. There are plans to incorporate this feature into the model in the future [27].

E. Mixed Finishes – Thin Sn Against Ag:

To test the model in a different way, an Ag cap was mated to a thin Sn coupon – adding another level of complexity. The model results show a correlation between the measured median values and the model analysis with the 'threshold' applied (Figure 17). Even though only one of the mating surfaces has an inherent oxide film, the 'threshold' is applied symmetrically across the a-spot areas to compensate for the

single oxide film as it was in the thin Sn against thin Sn analysis.

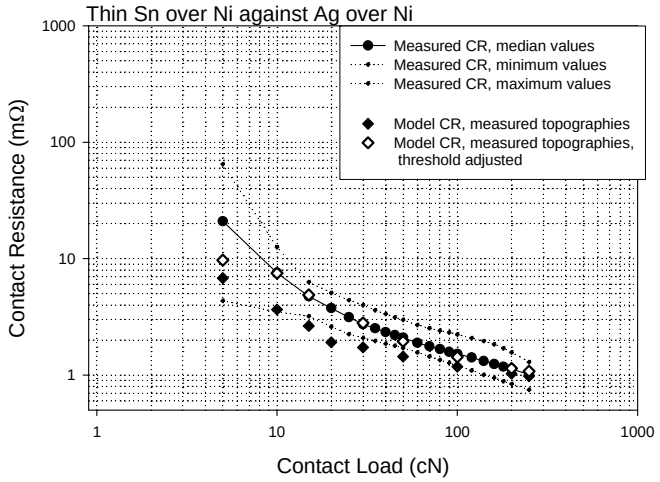

Figure 17: Measured contact resistance data as compared to model results for a thin Sn against Ag contact interface.

IV. CONCLUSIONS

The model results show a good correlation to measured 'real' world data for several contact finishes of interest. At the lower loads, both the measured and model results exhibit a 'knee' in the data. The 'knee' in the curve has been correlated to how the contact a-spot distribution develops as the load is increased; a function of the qualities of the two surfaces coming into contact.

From this evaluation, several possible adaptations to the model would be to:

- Incorporate alternate hardening behaviors into the a-spot interface development portion of the model.
- Improve the ability of the model to simulate material flow into the spaces around the a-spot junctions.
- Develop a contact heating/de-rating function for the 'Electro-Solver': to simulate potential softening of asperity junction material resulting from heat caused by current flow.
- Investigate incorporating a way to compensate for various surface films.

REFERENCES

[1] R. Holm, "Electric Contacts, Theory and Application," 4. Aufl., Springer Verlag, 1967/1999.

[2] H. Hertz, "Über die Berührung fester elastischer Körper. Verhandlungen des Vereins zur Beförderung des Gewebefleisses," 1882.

[3] H. S. Fluss, "Hertzian Stress as a Predictor of Contact Reliability," Connection Technology. Dec. 1990, pp 12 – 19.

[4] R. Mrockowski, "Concerning 'Hertz Stress' as a Connector Design Parameter," Proceedings of the 24th International Institute of Connector and Interconnection Technology, Oct. 1991, pp 327 - 336.

[5] J. A. Greenwood, "Constriction Resistance and the Area of Real Contact," British J. Appl. Phys., Vol. 17, 1966, pp 1621 – 1632.

[6] S. Kucharski, T. Klimczak, A. Polijaniuk, J. Kaczmarek, "Finite Elements Model for the Contact of Rough Surfaces," Wear, 177 (1994), pp 1-13.

[7] K. Komvopoulos, D. H. Choi, "Elastic Finite Element Analysis of Multi-Asperity Contact," Journal of Tribology, October 1992, vol. 114, pp 823 – 831.

[8] M. Leidner, H. Schmidt., H. Schlaak, "Simulation elektrischer und mechanischer Kennwerte von Steckverbinder Kontaktpunkten," Albert Keil Kontaktseminar, Vol 19, 2007, pp 211 – 220.

[9] M. Leidner, M. Myers, H. Schmidt, H. Schlaak., "A New Simulation Approach to Characterizing the Mechanical and Electrical Qualities of a Connector Contact", ICEC 2008 proceedings, June 2008, pp 165 – 170.

[10] G. S. P. Miller, "The Definition and Rendering of Terrain Maps," SIGRAPH 1986: Proceedings of the 13th Annual Conference on Computer Graphics and Interactive Techniques, Vol. 20, 1986, pp 39 - 48.

[11] M. Ausloos, D. H. Berman, "Multivariate Weier-Strass Mandelbrot Function," Proceedings of the Royal Society of London, Vol. 400, 1985, pp 331 – 350.

[12] Y. Z. Hu, K. Tonder., "Simulation of 3-D Random Surface by 2-D Filter and Fourier Analysis," Int. J. of Mach. Tools Maufact., Vol. 32, 1992, pp 82 – 90.

[13] N. Patir, "Numerical Procedure for Random Generation of Rough Surfaces," WEAR, Vol. 47, 1978, pp 263 – 277.

[14] S. Cai, B. Bushan, "Three Dimensional Dry/Wet Contact Analysis of Multilayered Elastic/Plastic Solids with Rough Surfaces," Journal of Tribology, 2006, *128*, pp. 18 – 31.

[15] K. L. Johnson, "Contact Mechanics," Cambridge University Press, 1985, 9.

[16] S. Liu, Q. Wang, "Studying Contact Stress Fields Caused by Surface Tractions With a Discrete Convolution and Fast Fourier Transform Algorithm," Transactions of the ASME, Vol. 124, 2002, pp 36 – 45.

[17] T. C. O'Sullivan, R. B. King, "Sliding Contact Stress Field Due to a Spherical Indenter on a Layered Elastic Medium," ASME J. Tribol., 1988, 110, pp. 235 – 240.

[18] I. A. Polonsky, L. M. Kerr, "A New Numerical Method for Solving Rough Contact Problems Based On The Multi-Level Multi-Summation and Conjugate Gradient Technique," WEAR, Vol. 231, 1999, 206 – 219.

[19] E. Rabinowicz, "Friction and Wear of Materials," John Wiley and Sons, Inc., – 1964.

[20] W. H. Abbott, "Materials, Environment, Motion, and Electrical Contact Failure Mechanisms," Proceedings of the 35th HOLM conference, 1989, pp 3 – 11.

[21] T. E. Graedel, "Corrosion Mechanisms for Silver Exposed to the Atmosphere", J. Electrochemical Society, Vol. 139, No. 7, 1992, pp 1963 – 1970.

[22] H. Schlaak, "Potentials and Limits of Micro-Electromechanical Systems for Relays and Switches," Proceedings of the 21st ICEC conference, September 2002, pp 9-12.

[23] J. Schimkat, "Grundlagen und Modelle zur Entwicklung und Optimierung von Silizium-Mikrorelais," Ph.D dissertation, TU Berlin, D83, 1996.

[24] K. Willner, "Elasto-Plastic Normal Contact of Three-Dimensional Fractal Surfaces Using Halfspace Theory," Transactions of the ASME - F - Journal of Tribology. 126, 2004, pp 28 – 33.

[25] Williamson, "The Microworld of the Contact Spot," Proceedings of the 27th HOLM conference, 1981, pp 1-10.

[26] H. Tian, N. Saka, "Finite Element Analysis of an Elastic-Plastic Two Layer Half-Space: Sliding Contact," Wear, Vol. 148, 1991, pp261- 285.

[27] Y. P. Chiu, "On the Stress Field due to Initial Stress in a Cuboidal Surrounded by an Infinite Half Space," J. Appl. Mech., Vol. 44, 1977, pp. 387 – 390.